ACS NANO

Cite This: ACS Nano 2019, 13, 5485−5492

www.acsnano.org

ARTICLE

Altering the Properties of Graphene on Cu(111) by Intercalation of Potassium Bromide

Mathias Schulzendorf,[†] Antoine Hinaut,[†] Marcin Kisiel,[†] Res Jöhr,[†,§] Rémy Pawlak,[†] Paolo Restuccia,[‡] Ernst Meyer,[†] Maria Clelia Righi,*[,‡] and Thilo Glatzel*[,†]

[†]Department of Physics, University of Basel, Klingelbergstr. 82, 4056 Basel, Switzerland

[‡]Dipartimento di Scienze Fisiche, Informatiche e Matematiche, Università di Modena e Reggio Emilia, Via Campi 213/A, 41125 Modena, Italy

[§]Lehrstuhl für Angewandte Physik and Center for Nanoscience, Ludwig-Maximilians-University, Amalienstr. 54, 80799 Munich, Germany

Supporting Information

ABSTRACT: **The catalytic growth on transition metal surfaces provides a clean and controllable route to obtain defect-free, monocrystalline graphene. However, graphene's optical and electronic properties are diminished by the interaction with the metal substrate. One way to overcome this obstacle is the intercalation of atoms and molecules decoupling the graphene and restoring its electronic structure. We applied noncontact atomic force microscopy to study the structural and electric properties of graphene on clean Cu(111) and after the adsorption of KBr or NaCl. By means of Kelvin probe force microscopy, a change in graphene's work function has been observed after the deposition of KBr, indicating a changed graphene−substrate interaction. Further measurements of single-electron charging events as well as X-ray photoelectron spectroscopy confirmed an electronic decoupling of the graphene islands by KBr intercalation. The results have been compared with density functional theory calculations, supporting our experimental findings.**

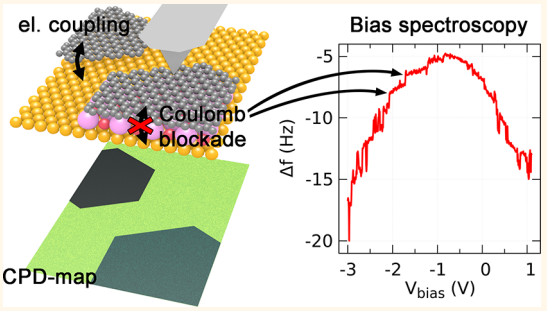

KEYWORDS: *graphene, KBr, intercalation, nc-AFM, KPFM, DFT, Coulomb blockade*

The intercalation of atoms or molecules between two-dimensional (2D) materials and the host substrate is of crucial importance for tuning their physical properties. One of the most studied and discussed 2D materials is graphene,[1,2] a single atom thick layer of sp^2-bonded carbon atoms arranged in a honeycomb lattice structure. Often it is prepared by chemical vapor deposition on metal surfaces such as Cu foils,[3] Ir, or Ru single-crystal surfaces[4,5] or on SiC(0001) by thermal decomposition of the SiC surface at increased temperatures.[6] The interaction of the graphene with these substrates, however, diminishes some of the special physical properties. For instance, interface states are induced by the presence of this coupling. These states, in turn, cause a high electron doping level in the graphene and serve as atomic scattering centers for charge carriers, which reduce the high-quality transport properties of graphene.[7,8] For the preparation of devices, a sophisticated transfer using several wet chemistry processes is required to deposit the graphene layers onto SiO_2 or other insulating substrates such as hexagonal boron nitride. However, these transfer methods cause contamination and defects.[9,10] Therefore, strategies to electrically decouple graphene from the substrate while maintaining sufficient adhesion and cleanness are explored. Moreover, tuning the parameters of the 2D layers by the substrate gating or even stacking of multiple different 2D materials is envisioned to result in advanced functional devices.[11−13]

An attractive route to address these challenges at the graphene/substrate interface is to intercalate atomic or molecular species. Similar to graphite intercalation compounds, in which the intercalation of different atoms between multiple graphite layers are changing the material characteristics,[14,15] it has been shown that a wide variety of atomic intercalants such as Eu,[16] H,[4] K,[17] Cs,[18] and others[19] also influence the physical properties of the 2D overlayer. For the case of Ir(111)

Received: January 11, 2019
Accepted: April 14, 2019
Published: April 15, 2019

DOI: 10.1021/acsnano.9b00278
ACS Nano 2019, 13, 5485−5492

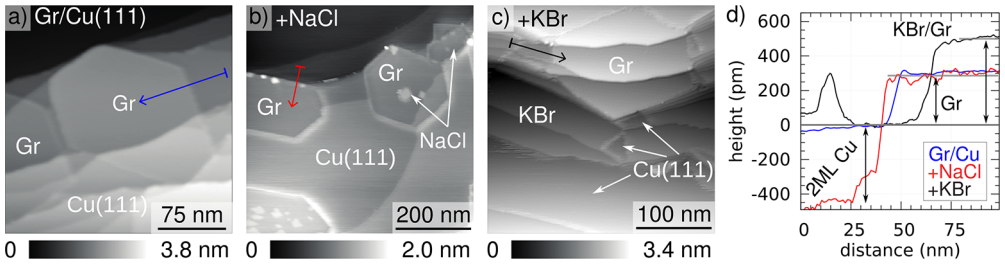

Figure 1. Topographic images of the graphene-covered Cu(111) surface before and after additional deposition of an alkali halide. (a) Cu(111) surface after growth of graphene by chemical vapor deposition. (b) After deposition of NaCl and subsequent annealing at 300 °C. NaCl is found in the form of islands on top of and next to graphene hexagons. (c) After deposition of KBr and annealing at 150 °C. The KBr appears as carpets that intercalate with the graphene. (d) Line profiles along the blue, red, and black arrows that support KBr intercalation.

substrates, this was also verified theoretically.[20,21] On Ru(0001), epitaxial graphene was decoupled by a stepwise intercalation of silicon and oxygen and the eventual formation of a SiO_2 layer between the graphene and the metal.[5] Another attractive surface for graphene preparation is SiC(0001), where hydrogen intercalation can break covalent bonds between the interfacial carbon-rich layer and the SiC substrate to transform it into a purely sp^2-bonded sheet of graphene.[22] Furthermore, alkali metal adsorption and intercalation have been used extensively to study the effects of electron doping.[23,24] A review of these transfer doping and intercalation experiments was summarized by Starke and co-workers.[25] However, the exact mechanism of the intercalation process is not yet clear, and different mechanisms such as the diffusion of the intercalant through atomic defects, open edges, or domain boundaries have been discussed intensively.[26,27]

Here, we will experimentally and theoretically show the intercalation of KBr between graphene and a Cu(111) surface. The atomically clean graphene sheets of well-controlled size and separation are prepared under ultrahigh vacuum (UHV) conditions upon annealing close to the melting point of the Cu(111) substrate. The (111) surfaces generally allow for a weak binding of the graphene layer to the metal substrates, resulting in a uniform graphene growth due to high diffusion and improved adsorption of carbon-containing species.[28,29] Among them, the Cu(111) surface is the most relevant as commercially used polycrystalline copper foils with a predominant (111) orientation are known to enhance the graphene quality.[30] We will show evidence for the uniform intercalation of a single KBr layer in graphene grown on such Cu(111) single-crystal surfaces and compare experimental and theoretical results with NaCl.

RESULTS AND DISCUSSION

Structural and electronic properties of graphene (Gr)/Cu(111) were investigated by atomic force microscopy in noncontact mode (nc-AFM) and Kelvin probe force microscopy (KPFM) experiments performed at room temperature (RT). These advanced scanning probe techniques allow one to measure structural and electronic surface properties with very high accuracy.[31−33] Here, in particular, the influence of postgrowth deposition and annealing of KBr and NaCl was analyzed in detail. Figure 1 shows three large-scale topographic images of the (a) Gr/Cu(111), (b) Gr/Cu(111) + NaCl, and (c) Gr/Cu(111) + KBr surfaces taken at RT with compensated contact potential difference (CPD).[34] In all measurements, the graphene islands with a size in the range of 150 nm in diameter have a clear hexagonal shape partly overgrowing Cu step edges. The identification of the different areas on these surfaces can be done by the structural appearance but is straightforward by using the respective KPFM data presented and discussed below (see Figure 2). A direct comparison of CPD and topography is presented in Figure S1 of the Supporting Information.

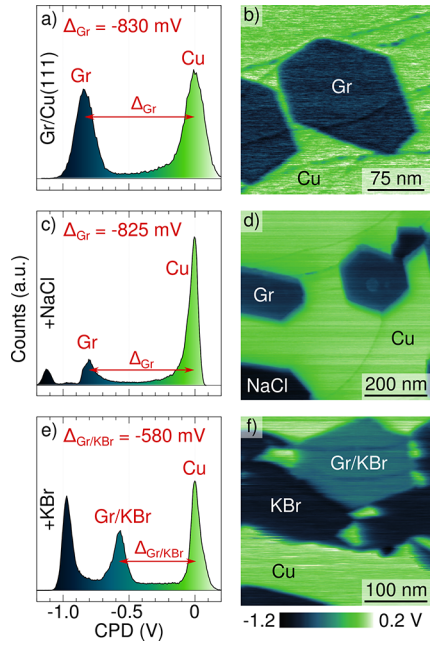

Figure 2. Normalized histograms (left column) of KPFM images (right column) taken simultaneously with the topographic images shown in Figure 1. Δ refers to the difference in surface potential of the respective graphene islands and Cu(111) (highlighted in red). The different materials can clearly be distinguished.

Deposition of NaCl onto a Gr/Cu(111) sample at RT and subsequent annealing at 300 °C resulted in small square-like islands and clusters on top of the hexagonal graphene flakes as well as NaCl single-layer islands that were generally attached to the graphene. Examples of both cases are marked by white arrows in the upper right of Figure 1b. A further annealing step at 400 °C resulted in a clean appearance of the Gr/Cu(111) system without edge decoration, square islands, or extended NaCl carpets (measurements not shown but similar to Figure 1a). As the sublimation temperature of NaCl is equal to or higher than about 470 °C, we expect the NaCl to diffuse and form larger crystals elsewhere on the surface.

DOI: 10.1021/acsnano.9b00278
ACS Nano 2019, 13, 5485−5492

Upon evaporation of KBr and postdeposition annealing at 150 °C, as presented in the nc-AFM measurement in Figure 1c, a different topography was observed. Large extended monolayer islands of KBr have been observed with small discontinuities uncovering the bare Cu(111) surface; some are marked by white arrows in Figure 1c. Although boundaries are clearly visible at these interfaces, the edge between KBr and the graphene flake appeared to be smooth. No small KBr islands were found on top of the hexagonal graphene flakes nor on top of extended KBr carpets.

To clarify the differences between the three systems, line profiles to determine the step height of graphene with respect to copper were taken and presented in Figure 1d. Because all of the measurements have been done with activated CPD compensation in the attractive interaction force regime, changes of the apparent height due to electrostatic forces are minimized. For the graphene on Cu(111) (blue curve), a height of 300 ± 20 pm was found. When NaCl was evaporated onto the surface, the step height of the hexagonal flakes remained unchanged (red curve), whereas the single- and second-layer NaCl islands have a height of 280 ± 20 pm. Note that the measured line profile appears higher by 450 ± 20 pm, which is the height of two atomic steps of copper, visible at the right edge of the flake with the line profile shown in Figure 1b. A clear difference in height was found when KBr was additionally deposited (Figure 1c) and annealed at 150 °C. The measured height of the graphene flakes increased to 500 ± 40 pm. An accurate measurement was, however, more difficult to obtain because most of the graphene flakes were surrounded by KBr islands. Whereas these height considerations already give a first hint for a clear distinction between the two alkali halide graphene systems, the changes in the simultaneously measured surface potential reveal an even more pronounced difference.

The hexagonal flakes are clearly distinguishable by their smaller work function compared to that of Cu(111), as can be observed in Figure 2a,b. A difference of $\Delta_{Gr} = -830 \pm 20$ mV was found for the CPD of bare graphene with respect to Cu(111). Assuming a theoretical work function for Cu(111)[35] of $\Phi_{Cu(111)} = 5.19$ eV results in a work function for graphene of $\Phi_{Gr} = 4.36 \pm 0.02$ eV. This is in perfect agreement with the predicted value for weakly coupled and slightly n-doped graphene on Cu(111).[36]

The effect of the adsorption of NaCl on the work function of the system is shown in Figure 2c,d. The small hexagonal island at the bottom left has a work function difference to Cu(111) of $\Delta_{NaCl} = -1060 \pm 20$ mV, which is the value observed also for pure NaCl layers on Cu(111).[37] Therefore, and also based on the structural appearance (Figure 1b), the lower graphene flake appeared to be completely overgrown by NaCl. Also, the small upper right island connected to a graphene flake shows a reduced CPD. For the graphene flakes, we noticed no change in the CPD as compared to the values measured on the bare Gr/Cu(111) system, with a difference equal to $\Delta_{Gr} = -825 \pm 20$ mV. A comparison of bias spectroscopy curves taken on the bare Cu(111) surface, a graphene flake, and a NaCl island is shown in Figure S2 of the Supporting Information.

Significant changes were found after the evaporation of KBr, presented in Figure 2e,f. Due to its structural appearance, the extended carpet can be identified as KBr with a $\Delta_{KBr} = -970 \pm 20$ mV. The discontinuities, as discussed for the topography, are areas of bare Cu(111) having fuzzy edges to the KBr carpets. These more fuzzy boundaries are also present at all other KBr edges, indicating a weak binding of the KBr layers to the substrate. The graphene islands now have a clearly reduced work function difference equal to $\Delta_{Gr/KBr} = -580 \pm 20$ mV. Compared to graphene on the clean Cu(111) surface, the work function of graphene increased by 250 mV to $\Phi_{Gr/KBr} = 4.61 \pm 0.02$ eV, a value comparable to that of free-standing graphene or with a slight p-doping.[36] To further elucidate on the changes after KBr deposition, moiré and atomic structure were resolved by high-resolution nc-AFM measurements on the graphene islands.

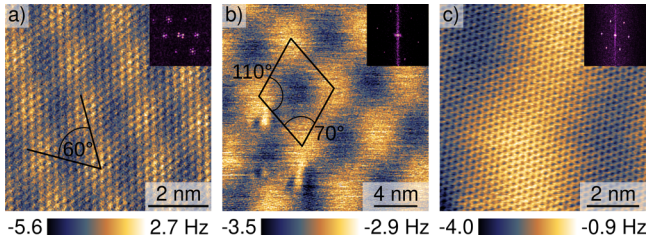

Figure 3. High-resolution images of the moiré and atomic structure for the graphene islands in bimodal AFM using the torsional frequency shift Δf_{tr}. (a) Moiré pattern for Gr/Cu(111) together with the periodicity of the graphene lattice. (b) New larger moiré pattern appears after deposition of KBr taken at the center of the graphene island presented in Figure 1c, which leaves the periodicity of the graphene lattice unchanged (c). The insets are the FFT images.

Figure 3 shows the torsional frequency shift signal which was measured in bimodal AFM mode, allowing for high-resolution measurements even on sensitive surfaces.[38,39] For bare graphene on Cu(111), the known moiré structure[40] was resolved, as shown in Figure 3a. The large hexagonal (60°) repeating pattern corresponds to the moiré structure with a lattice parameter of 1.9 nm and a height variation of 25 pm, whereas the small one is related to the periodicity of the graphene layer (≈245 ± 30 pm). The fast Fourier transform (FFT) shown in the upper right corner nicely resolves those two periodicities. Comparable structures have been found for the samples with additional NaCl. Figure 3b,c shows similar measurements of the torsional frequency shift in the presence of KBr taken at the center of the graphene island presented in Figure 1c. A clearly larger moiré structure with a periodicity of 7.0 nm and a height variation of 11 pm indicates a different binding mechanism of the graphene layer to the substrate, however, this time with an oblique lattice, as marked by the primitive unit cell shown in Figure 3b. The observed moiré pattern has not been measured nor theoretically predicted for graphene grown on Cu(111).[41] This larger periodicity and the weaker corrugation indicate a reduced compressive strain within graphene[42] and a weaker coupling to the substrate after adsorption of KBr. The second image in Figure 3c is a zoomed-in high-resolution image showing the perfect graphene lattice of the layer with a periodicity of ≈215 ± 30 pm, which is in good agreement with the value determined before and verifying that the KBr layer is not on top of the graphene layer.

The most striking arguments for a real decoupling of the graphene layer are, however, the charging features observed only for the KBr intercalated graphene islands, as presented in Figure 4, and known as Coulomb blockade effect.[43−47] Sixty-four bias spectroscopy curves (see also Figure S3 in the Supporting Information) have been measured along a line of

DOI: 10.1021/acsnano.9b00278
ACS Nano 2019, 13, 5485−5492

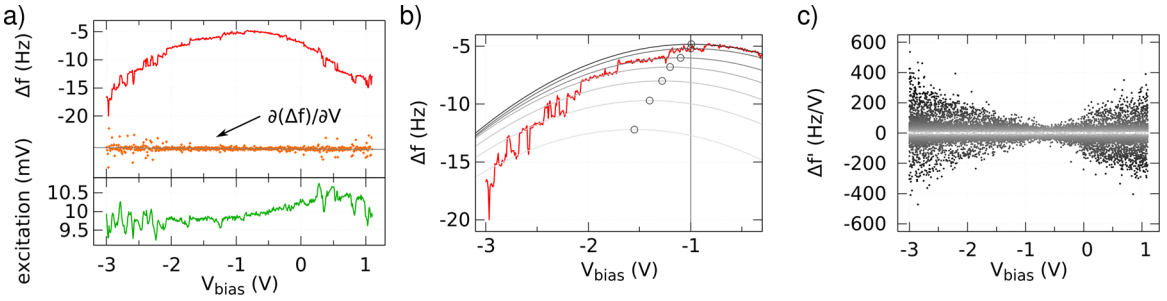

Figure 4. (a) Frequency shift Δf, derivative $f' = \partial(\Delta f)/\partial V$, and excitation signal of a bias spectroscopy measurement taken at the center of the graphene island of Figure 1c. (b) Fitting of the plateaus of the Δf curve showing the shift of the LCPD (circles) and the jumps between different charge states. (c) Derivatives of all 64 frequency shift curves on the same Gr/KBr/Cu(111) system taken along a line of 12 nm across the moiré structure and at the center of the graphene island. The contrast of the data points is adopted to the absolute value of $\Delta f'$.

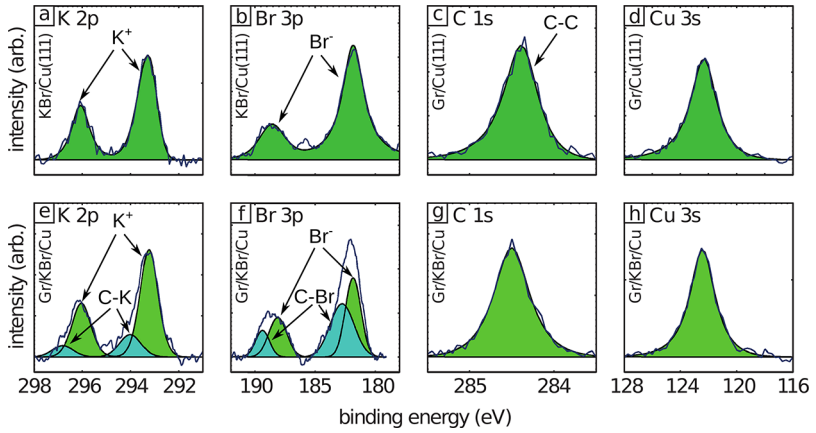

Figure 5. K 2p and Br 3p peaks measured by XPS for KBr only on Cu(111) in (a,b), C 1s and Cu 3s for graphene on Cu(111) in (c,d), and K 2p, Br 3p, C 1s, and Cu 3s for the intercalated system Gr/KBr/Cu(111) (e−h). Second peaks emerged for K and Br and are related to the intercalation.

12 nm across the moiré structure at constant height at the center of the graphene island presented in Figure 1c. All curves show regular jumps in the forward and backward frequency shift data. Those jumps are related to single-electron charging events of the graphene layer induced by electron tunneling from the substrate through the decoupling KBr layer. One of these bias spectroscopy curves is presented with its derivative and the simultaneously measured excitation signal in Figure 4a. The jumps in the frequency shift signal are always accompanied by a sudden rise of the excitation signal, again a known feature of single-electron charging.[43,48] In the case of bare graphene on Cu(111) and for islands with deposited NaCl, these jumps are not present and the shape of the bias spectroscopy curves follows perfectly the expected parabolic dependence (see Figures S2 and S4). Each jump is related to a shift of the local CPD (LCPD) (shown in Figure 4b) as well as a change in the capacitance gradient and, therefore, results in a modified quadratic dependence of the frequency shift *versus* bias voltage.

In general, two requirements have to be fulfilled for the Coulomb blockade observation. First, the charging energy $E_C = q^2/C_{tot}$, where q is the elementary charge and C_{tot} the total capacitance of the AFM tip and Cu(111) circuit, has to be larger than the thermal energy $k_BT \approx 25$ meV. Second, the tunneling resistance R_t of the Gr/KBr/Cu(111) junction must be larger than the resistance quanta $h/q^2 = 25.8$ KΩ.[49] Here, the overall circuit is built up by two capacitors in series: one of tip/Gr (C_{tip}) and the other of Gr/Cu(111) (C_{Gr}) as well as R_t connected in parallel to C_{Gr}. This results in the total capacitance $\frac{1}{C_{tot}} = \frac{1}{C_{Gr}} + \frac{1}{C_{tip}}$. C_{Gr} can be determined by using a standard parallel plate capacitor model with the area of this particular graphene flake ($A_{Gr} \approx 0.19\ \mu m^2$), the distance to the substrate ($d_{Gr/Cu} \approx 500$ pm), and an estimated value for the relative dielectric constant of a monolayer of KBr ($\epsilon_{KBr} = 4.87$) to be in the fF regime. In contrast, the capacitance of the tip/Gr system can be estimated by using a sphere over a plate capacitance model[50] or the Hudlet model of a conical electrode above a plate[51,52] to be in the aF regime. This indicates that the energy of the Coulomb blockade is controlled dominantly by the tip/Gr capacitance and is, therefore, mainly related to the effective tip radius and the tip−sample distance. The bias spectroscopy in Figure 4a shows regular jumps with a periodicity of approximately 300 mV for altering the charge of the graphene layer by one electron, resulting in an effective (electrostatic) tip radius of ≈30 nm, which is a reasonable value for the used tip.[53] The expression given by Stomp *et al.*[43] for the charging force of InAs quantum dots is verified in Figure 4c, where we present all 64 measurements of frequency shift derivatives on the Gr/KBr/Cu(111) system taken at room temperature (please note that to calculate $\partial(\Delta f)/\partial V$, we use the gradient approximation $\Delta f = \frac{f_0}{2k}\frac{\partial F}{\partial z}$):

$$\partial(\Delta f)/\partial V = \frac{f_0}{2k}\left(\frac{\partial C_{tot}}{\partial z}\right)^2\left(V_{DC} - \frac{q}{C_{Gr}}\right)$$

DOI: 10.1021/acsnano.9b00278
ACS Nano 2019, 13, 5485−5492

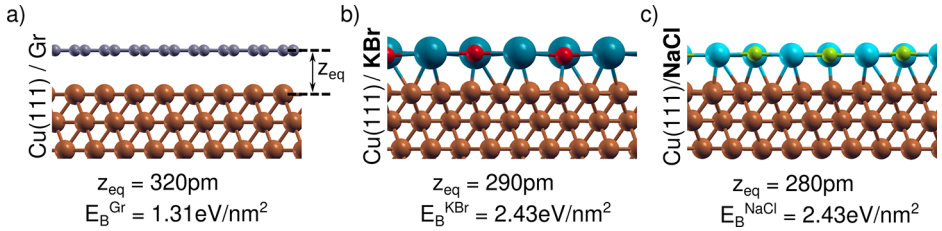

Figure 6. Optimized structures of graphene (a), KBr (b), and NaCl (c) on the Cu(111) surface. Alkali atoms are colored in light blue, with K presenting a larger atomic radius than Na, whereas Br and Na are colored in red and green, respectively. The calculated binding energies, E_B, and adsorption distances, z_{eq}, are reported in each panel.

Here, z is the tip−sample distance, f_0 is free cantilever frequency, and k is the spring constant. A linear increase of this jump intensity with larger bias voltages is observed as predicted by the simple formula. Due to thermal activation, the distances between subsequent charging events are, however, not all equidistant as visible in the single curve in Figure 4a. All of these measurements have a clear signature of Coulomb blockade phenomena, impossible without a reasonable decoupling ($R_t \gg 25.8$ kΩ) of the graphene layer from the Cu(111) substrate.

Finally, photoelectron spectroscopy measurements are also a well-known method to verify intercalation processes.[54,55] Therefore, the changes found for the adsorption of KBr were further corroborated by means of X-ray photoelectron spectroscopy (XPS) at the PEARL beamline of the Swiss Light Source[56] and are presented in Figure 5. The samples have been prepared *in situ* similar to the preparation of the samples for the AFM measurements, and scanning tunneling microscopy was used to verify successful surface preparation. Clean Cu(111) samples with KBr (Figure 5a,b) and graphene (Figure 5c,d) have been compared at RT with the intercalated sample. As shown in Figure 5a, the typical K 2p spectrum has two clearly spaced spin−orbit components at binding energies of 293.3 eV (K $2p_{3/2}$) and 296.0 eV (K $2p_{1/2}$) as well as the Br spectra at binding energies of 181.8 eV (Br $3p_{3/2}$) and 188.1 eV (Br $3p_{1/2}$). The observed peak positions correspond to the ionized materials as the samples have been prepared in an oxygen-free environment.[57,58] The C 1s spectra comprise a major peak at 284.4 eV, which is associated with the C−C bonding and is consistent with sp^2-hybridized graphite carbon,[59] again without the influence of oxygen, and a major peak at 122.2 eV for Cu 3s. Whereas the C 1s peak moves upon KBr intercalation to slightly higher energies (≈100 meV), the Cu 3s stays within the limit of resolution at the same position. This small but not negligible shift in the binding energy might be a result of positive charging of the surface upon XPS measurements, which correlates well with the observed decoupling of the graphene. However, the observed shift is weak due to spatial averaging in the XPS measurements and a relatively low density of graphene islands on the surface. Furthermore, second peaks at higher binding energies were also found for both K 2p (294.0 and 296.8 eV) and Br 3p (183.8 and 189.4 eV), as shown in Figure 5e,f. These additional peaks are comparable to results already observed beforehand for pure potassium and bromine interaction with graphene,[57,58] indicating a different binding configuration of the carbon, bromine, and potassium atoms, corresponding to C−Br (C−K) bonds and Br^- (K^+) species, respectively. These results support the successful intercalation of KBr between Gr/Cu(111) and are, for example, comparable to the intercalation of K in multiwalled carbon nanotubes or graphene by metallic potassium[57,59] and the binding of bromine to multiwalled carbon nanotubes or graphene.[58,60]

To theoretically corroborate the intercalation process and the obvious difference of NaCl and KBr, we performed density functional theory (DFT) calculations. In a first set of calculations, we studied the adsorption of graphene and alkali halides (AH) adsorbed on Cu(111), and the optimized structures at 0 K are shown in Figure 6. AH adsorption on copper turned out to be more energetically favorable than graphene adsorption: the calculated binding energies and distances are, in fact, in the range of chemisorption for AH and of physisorption for graphene. This result suggests that when Gr and AH layers are stacked on copper, the layer that will most likely be in contact with the substrate is AH. This was confirmed by a direct comparison of the total energies of Gr/AH/Cu(111) and AH/Gr/Cu(111) structures, the former being more stable.

The optimized geometry of the Gr/AH/Cu(111) structure is shown in Figure 7 (the AH/Gr/Cu(111) structure is not shown as it is unstable). We can observe that intercalation produces an enhancement of the buckling within the KBr layer: It increases from 20 pm observed for KBr adsorption (Figure 6b) to 45 pm for KBr intercalation (Figure 7a). This effect is absent in NaCl, whose adsorption geometry does not seem to be affected by the presence of graphene. The larger distortion of the KBr structure upon intercalation is most likely caused by the strong interaction between K and graphene. This interaction stabilizes the Gr/KBr/Cu(111) structure with respect to separate adsorptions of Gr/Cu(111) + KBr/Cu(111). The binding energy of graphene increases, in fact, from 1.31 eV/nm^2 on bare copper to 1.37 eV/nm^2 on KBr/Cu(111). The situation is opposite for NaCl, where intercalation does not produce an energy gain but an energy

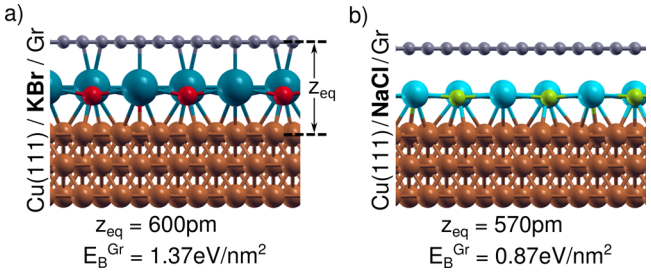

Figure 7. Optimized configurations for alkali halide intercalation between graphene and the Cu(111) substrate. The binding energy of graphene on the KBr/Cu(111) (a) and NaCl/Cu(111) (b) substrates is reported along with the graphene equilibrium distance relative to the Cu(111) surface.

DOI: 10.1021/acsnano.9b00278
ACS Nano 2019, 13, 5485−5492

cost, with the binding energy of graphene on NaCl/Cu(111), 0.87 eV/nm^2, lower than that on bare copper.

Therefore, we may speculate that at the temperatures present during alkali halide deposition and the postannealing step, graphene flakes weakly bonded on the Cu(111) surface can diffuse and adhere more steadily on newly formed KBr islands, whereas they will not cover NaCl islands because the binding is weaker than that on bare metal surfaces. Another possibility might be the penetration of KBr through defects and step edges of the graphene and the formation of the intercalated layer. In any case, the DFT energetics are consistent with the experimental observation of KBr intercalation between graphene and the copper substrate, which is not observed for NaCl.

CONCLUSIONS

In conclusion, we demonstrated the KBr intercalation and electrical decoupling of extended graphene islands from Cu(111) single-crystal surface experimentally and theoretically, which allows one to apply this method to other systems such as graphene nanoribbons or even adapt it to different 2D materials. The possibility to study single-electron charging at room temperature may be used as an efficient tool for surface analysis with a high spatial and energetic resolution that will allow for tuning optical, magnetic, and eventually tribological[61] properties of graphene. Appropriate electrical decoupling of graphene impacts not only fundamental research but also technological applications.

METHODS

Sample Preparation. The single-layer graphene flakes were grown in UHV on a freshly prepared Cu(111) single-crystal surface. The Cu(111) surface was prepared by several cycles of Ar^- ion sputtering (800−1000 eV, 3×10^{-6} mbar Ar pressure and 10−20 min) and annealing (500−600 °C, 10−20 min) cycles. Graphene was prepared according to Gao *et al.*[40] by repeated high-temperature flashes in UHV. The sample was first heated to 300 °C while the precursor gas, ethylene (C_2H_4), was dosed directly to the sample through a nozzle at a distance of 2−10 mm. The chamber pressure during the process was 4×10^{-6} mbar, however, with presumably a much higher local ethylene pressure at the sample surface. For one flash, the sample temperature was ramped up at 600 °C/s to 950 °C and held for 1 min. Afterward, the sample was cooled to 300 °C. The flashing process was repeated several times (typically four times), and before the last cool down process, the ethylene supply was stopped. If necessary, the sample was annealed at 600 °C to get rid of residual contaminations.

NaCl and KBr were thermally evaporated from a quartz crucible in UHV to the Gr/Cu(111) sample at evaporation temperatures of 470 and 410 °C, respectively. These deposition temperatures resulted in an average rate of 0.23 Å/min. By using different sample temperatures, typically 70−175 °C, an optimal island formation was achieved.

nc-AFM Measurements. AFM measurements were performed without breaking the UHV for sample transfer in a home-built microscope using beam deflection detection with a bandwidth of 3 MHz. Standard topographic measurements were performed by using the first flexural mode of the cantilever (PPP-NCL, nanosensors) with a center frequency of f_{1st} = 165 kHz and an amplitude of A_{1st} = 6 nm. The typical quality factor of the cantilevers in UHV is Q_{1st} = 32 000. KPFM was done in the so-called FM-KPFM mode at the first flexural mode using an AC excitation voltage of V_{AC} = 1 V and f_{AC} = 210 Hz. AC and DC biases were applied to the sample so that a smaller CPD corresponded to a smaller sample work function.[34] Bimodal experiments were also conducted by using the first PLL to control the tip sample distance coupled to a second PLL to drive the first torsional oscillation mode with values typically around f_{tr} = 1 MHz, an amplitude of A_{tr} = 50 pm, and quality factor of Q_{tr} = 60 000.

XPS Measurements. XPS measurements were performed at the X03DA beamline (PEARL endstation)[56] at the SLS synchrotron radiation facility (Villigen, Switzerland). The samples were prepared *in situ* with a process similar to that described above for the AFM measurements without any air exposure. The surface of these samples was analyzed prior to the XPS measurements by scanning tunneling microscopy, showing results comparable to the ones presented in Figure 1. All XPS spectra were taken at normal emission and were recorded at room temperature with a photon energy of 800 eV.

Computational Method. DFT calculations were performed within the local density approximation. The electronic wave functions are expanded in plane waves and the ionic species described by ultrasoft pseudopotentials.[62] On the basis of test calculations for bulk copper, we chose a kinetic energy cutoff for the wave function (charge density) equal to 30 Ry (240 Ry). Because there is a significant mismatch between the lattice parameters of the considered adsorbate layers and copper, we adopted metal slabs of different in-plane sizes to reduce the strain of the adlayer: graphene on copper was modeled by a (1 × 1)-Cu(111) hexagonal cell, where the mismatch was about 4%; the KBr/Cu(111) (NaCl/Cu(111)) system was modeled by a rectangular slab of $5 \times 3\sqrt{3}$ ($(7 \times 4\sqrt{3})$) in-plane size (each rectangular unit cell is composed by two hexagonal (1 × 1) cells) and 2% (5%) associated mismatch. The Brillouin zone sampling of the supercells used to model the Gr/Cu(111), KBr/Cu(111), and NaCl/Cu(111) systems are realized by means of 10 × 10, 2 × 2, and 1 × 1 Monkhorst−Pack grids. In order to isolate the adsorbate systems from their periodic replicas along the z-direction, a vacuum region of 1.4 nm was included in the supercell. The binding energy of an adsorbed layer to the substrate was calculated as $E_B = -(E_{tot} - E_{layer} - E_{sub})/A$, where E_{tot} is the energy of the adsorbate system, and E_{layer} and E_{sub} are the energies of the isolated layer and substrate, respectively. A is the supercell in-plane area.

ASSOCIATED CONTENT

Supporting Information

The Supporting Information is available free of charge on the ACS Publications website at DOI: 10.1021/acsnano.9b00278.

Direct comparison of topography and CPD measurements, an overview of all 64 bias spectroscopy curves, and bias spectroscopy curves of Gr/NaCl, Gr, and pure Cu(111) (PDF)

AUTHOR INFORMATION

Corresponding Authors

*E-mail: mcrighi@unimore.it.

*E-mail: thilo.glatzel@unibas.ch.

ORCID

Antoine Hinaut: 0000-0002-2608-2564

Rémy Pawlak: 0000-0001-8295-7241

Paolo Restuccia: 0000-0002-0419-723X

Ernst Meyer: 0000-0001-6385-3412

Thilo Glatzel: 0000-0002-3533-4217

Notes

The authors declare no competing financial interest.

ACKNOWLEDGMENTS

The authors thank M. Muntwiler and J. Zhang from the Swiss Light Source (X03DA, PEARL) for beamline support as well as the Swiss National Science Foundation (SNSF), the Swiss Nanoscience Institute (SNI), and the University of Basel for funding. M.C.R. thanks Materials Design at the Exascale (MaX) GA 676598 H2020 EINFRA-2015-1 and the University

DOI: 10.1021/acsnano.9b00278
ACS Nano 2019, 13, 5485−5492

of Modena and Reggio Emilia through the Fondi di Ateneo per la Ricerca (FAR) 2016 project. The authors thankfully acknowledge CINECA (Consorzio Interuniversitario del Nord est Italiano Per il Calcolo Automatico) for supercomputing resources through the project Italian SuperComputing Resource Allocation (ISCRA) B StressRx.

REFERENCES

(1) Novoselov, K. S.; Geim, A. K.; Morozov, S. V.; Jiang, D.; Zhang, Y.; Dubonos, S. V.; Grigorieva, I. V.; Firsov, A. A. Electric Field Effect in Atomically Thin Carbon Films. *Science* **2004**, *306*, 666−669.

(2) Novoselov, K. S.; Geim, A. K.; Morozov, S. V.; Jiang, D.; Katsnelson, M. I.; Grigorieva, I. V.; Dubonos, S. V.; Firsov, A. A. Two-Dimensional Gas of Massless Dirac Fermions in Graphene. *Nature* **2005**, *438*, 197−200.

(3) Li, X.; Cai, W.; An, J.; Kim, S.; Nah, J.; Yang, D.; Piner, R.; Velamakanni, A.; Jung, I.; Tutuc, E.; et al. Large-Area Synthesis of High-Quality and Uniform Graphene Films on Copper Foils. *Science* **2009**, *324*, 1312−1314.

(4) Langer, T.; Förster, D. F.; Busse, C.; Michely, T.; Pfnür, H.; Tegenkamp, C. Sheet Plasmons in Modulated Graphene on Ir(111). *New J. Phys.* **2011**, *13*, 053006.

(5) Lizzit, S.; Larciprete, R.; Lacovig, P.; Dalmiglio, M.; Orlando, F.; Baraldi, A.; Gammelgaard, L.; Barreto, L.; Bianchi, M.; Perkins, E.; et al. Transfer-Free Electrical Insulation of Epitaxial Graphene from its Metal Substrate. *Nano Lett.* **2012**, *12*, 4503−4507.

(6) Mishra, N.; Boeckl, J.; Motta, N.; Iacopi, F. Graphene Growth on Silicon Carbide: A Review. *Phys. Status Solidi A* **2016**, *213*, 2277−2289.

(7) Xu, Z.; Buehler, M. J. Interface Structure and Mechanics Between Graphene and Metal Substrates: A First-Principles Study. *J. Phys.: Condens. Matter* **2010**, *22*, 485301.

(8) Armbrust, N.; Güdde, J.; Höfer, U. Formation of Image-Potential States at the Graphene/Metal Interface. *New J. Phys.* **2015**, *17*, 103043.

(9) Liang, X.; Sperling, B. A.; Calizo, I.; Cheng, G.; Hacker, C. A.; Zhang, Q.; Obeng, Y.; Yan, K.; Peng, H.; Li, Q.; et al. Toward Clean and Crackless Transfer of Graphene. *ACS Nano* **2011**, *5*, 9144−9153.

(10) Goossens, A. M.; Calado, V. E.; Barreiro, A.; Watanabe, K.; Taniguchi, T.; Vandersypen, L. M. K. Mechanical Cleaning of Graphene. *Appl. Phys. Lett.* **2012**, *100*, 073110.

(11) Freitag, M. Nanoelectronics Goes Flat Out. *Nat. Nanotechnol.* **2008**, *3*, 455−457.

(12) Wang, X.; Zhi, L.; Müllen, K. Transparent, Conductive Graphene Electrodes for Dye-Sensitized Solar Cells. *Nano Lett.* **2008**, *8*, 323−327.

(13) Berger, C.; Song, Z.; Li, T.; Li, X.; Ogbazghi, A. Y.; Feng, R.; Dai, Z.; Marchenkov, A. N.; Conrad, E. H.; First, P. N.; et al. Ultrathin Epitaxial Graphite: 2D Electron Gas Properties and a Route Toward Graphene-Based Nanoelectronics. *J. Phys. Chem. B* **2004**, *108*, 19912−19916.

(14) Dresselhaus, M. S.; Dresselhaus, G. Intercalation Compounds of Graphite. *Adv. Phys.* **2002**, *51*, 1−186.

(15) Weller, T. E.; Ellerby, M.; Saxena, S. S.; Smith, R. P.; Skipper, N. T. Superconductivity in the Intercalated Graphite Compounds C_6Yb and C_6Ca. *Nat. Phys.* **2005**, *1*, 39−41.

(16) Schumacher, S.; Förster, D. F.; Rösner, M.; Wehling, T. O.; Michely, T. Strain in Epitaxial Graphene Visualized by Intercalation. *Phys. Rev. Lett.* **2013**, *110*, 086111.

(17) Bianchi, M.; Rienks, E. D. L.; Lizzit, S.; Baraldi, A.; Balog, R.; Hornekær, L.; Hofmann, P. Electron-Phonon Coupling in Potassium-Doped Graphene: Angle-Resolved Photoemission Spectroscopy. *Phys. Rev. B: Condens. Matter Mater. Phys.* **2010**, *81*, 041403.

(18) Petrović, M.; Šrut Rakić, I.; Runte, S.; Busse, C.; Sadowski, J. T.; Lazić, P.; Pletikosić, I.; Pan, Z.-H.; Milun, M.; Pervan, P.; et al. The Mechanism of Caesium Intercalation of Graphene. *Nat. Commun.* **2013**, *4*, 2772.

(19) Yurtsever, A.; Onoda, J.; Iimori, T.; Niki, K.; Miyamachi, T.; Abe, M.; Mizuno, S.; Tanaka, S.; Komori, F.; Sugimoto, Y. Effects of Pb Intercalation on the Structural and Electronic Properties of Epitaxial Graphene on SiC. *Small* **2016**, *12*, 3956−3966.

(20) Andersen, M.; Hornekær, L.; Hammer, B. Understanding Intercalation Structures Formed Under Graphene on Ir(111). *Phys. Rev. B: Condens. Matter Mater. Phys.* **2014**, *90*, 155428.

(21) Hasegawa, M.; Nishidate, K.; Hosokai, T.; Yoshimoto, N. Electronic-Structure Modification of Graphene on Ni(111) Surface by the Intercalation of a Noble Metal. *Phys. Rev. B: Condens. Matter Mater. Phys.* **2013**, *87*, 085439.

(22) Riedl, C.; Coletti, C.; Iwasaki, T.; Zakharov, A. A.; Starke, U. Quasi-Free-Standing Epitaxial Graphene on SiC Obtained by Hydrogen Intercalation. *Phys. Rev. Lett.* **2009**, *103*, 246804.

(23) Sandin, A.; Jayasekera, T.; Rowe, J. E.; Kim, K. W.; Buongiorno Nardelli, M.; Dougherty, D. B. Multiple Coexisting Intercalation Structures of Sodium in Epitaxial Graphene-SiC Interfaces. *Phys. Rev. B: Condens. Matter Mater. Phys.* **2012**, *85*, 125410.

(24) Ohta, T.; Bostwick, A.; Seyller, T.; Horn, K.; Rotenberg, E. Controlling the Electronic Structure of Bilayer Graphene. *Science* **2006**, *313*, 951−954.

(25) Starke, U.; Forti, S.; Emtsev, K.; Coletti, C. Engineering the Electronic Structure of Epitaxial Graphene by Transfer Doping and Atomic Intercalation. *MRS Bull.* **2012**, *37*, 1177−1186.

(26) Li, G.; Zhou, H.; Pan, L.; Zhang, Y.; Huang, L.; Xu, W.; Du, S.; Ouyang, M.; Ferrari, A. C.; Gao, H.-J. Role of Cooperative Interactions in the Intercalation of Heteroatoms Between Graphene and a Metal Substrate. *J. Am. Chem. Soc.* **2015**, *137*, 7099−7103.

(27) Markevich, A.; Jones, R.; Öberg, S.; Rayson, M. J.; Goss, J. P.; Briddon, P. R. First-Principles Study of Hydrogen and Fluorine Intercalation into Graphene-SiC(0001) Interface. *Phys. Rev. B: Condens. Matter Mater. Phys.* **2012**, *86*, 045453.

(28) Jeon, C.; Hwang, H.-N.; Lee, W.-G.; Jung, Y. G.; Kim, K. S.; Park, C.-Y.; Hwang, C.-C. Rotated Domains in Chemical Vapor Deposition-Grown Monolayer Graphene on Cu(111): An Angle-Resolved Photoemission Study. *Nanoscale* **2013**, *5*, 8210−8214.

(29) Gottardi, S.; Müller, K.; Bignardi, L.; Moreno-López, J. C.; Pham, T. A.; Ivashenko, O.; Yablonskikh, M.; Barinov, A.; Björk, J.; Rudolf, P.; et al. Comparing Graphene Growth on Cu(111) *versus* Oxidized Cu(111). *Nano Lett.* **2015**, *15*, 917−922.

(30) Wood, J. D.; Schmucker, S. W.; Lyons, A. S.; Pop, E.; Lyding, J. W. Effects of Polycrystalline Cu Substrate on Graphene Growth by Chemical Vapor Deposition. *Nano Lett.* **2011**, *11*, 4547−4554.

(31) Glatzel, T.; Hölscher, H.; Schimmel, T.; Baykara, M. Z.; Schwarz, U. D.; Garcia, R. Advanced Atomic Force Microscopy Techniques. *Beilstein J. Nanotechnol.* **2012**, *3*, 893−894.

(32) Glatzel, T.; Garcia, R.; Schimmel, T. Advanced Atomic Force Microscopy Techniques II. *Beilstein J. Nanotechnol.* **2014**, *5*, 2326−2327.

(33) Morita, S., Giessibl, F. J., Meyer, E., Wiesendanger, R., Eds. *Noncontact Atomic Force Microscopy*; Springer International Publishing, 2015.

(34) Sadewasser, S., Glatzel, T., Eds. *Kelvin Probe Force Microscopy: From Single Charge Detection to Device Characterization*; Springer International Publishing, 2018.

(35) Cook, B.; Russakoff, A.; Varga, K. Coverage Dependent Work Function of Graphene on a Cu(111) Substrate with Intercalated Alkali Metals. *Appl. Phys. Lett.* **2015**, *106*, 211601.

(36) Khomyakov, P. A.; Giovannetti, G.; Rusu, P. C.; Brocks, G.; van den Brink, J.; Kelly, P. J. First-Principles Study of the Interaction and Charge Transfer Between Graphene and Metals. *Phys. Rev. B: Condens. Matter Mater. Phys.* **2009**, *79*, 195425.

(37) Glatzel, T.; Zimmerli, L.; Koch, S.; Such, B.; Kawai, S.; Meyer, E. Determination of Effective Tip Geometries in Kelvin Probe Force Microscopy on Thin Insulating Films on Metals. *Nanotechnology* **2009**, *20*, 264016.

(38) Kawai, S.; Glatzel, T.; Koch, S.; Such, B.; Baratoff, A.; Meyer, E. Systematic Achievement of Improved Atomic-Scale Contrast *via*

DOI: 10.1021/acsnano.9b00278
ACS Nano 2019, 13, 5485−5492

Bimodal Dynamic Force Microscopy. *Phys. Rev. Lett.* **2009**, *103*, 220801.
(39) Kawai, S.; Glatzel, T.; Koch, S.; Such, B.; Baratoff, A.; Meyer, E. Ultrasensitive Detection of Lateral Atomic-Scale Interactions on Graphite (0001) *via* Bimodal Dynamic Force Measurements. *Phys. Rev. B: Condens. Matter Mater. Phys.* **2010**, *81*, 085420.
(40) Gao, L.; Guest, J. R.; Guisinger, N. P. Epitaxial Graphene on Cu(111). *Nano Lett.* **2010**, *10*, 3512−3516.
(41) Süle, P.; Szendrő, M.; Hwang, C.; Tapasztó, L. Rotation Misorientated Graphene Moiré Superlattices on Cu(111): Classical Molecular Dynamics Simulations and Scanning Tunneling Microscopy Studies. *Carbon* **2014**, *77*, 1082−1089.
(42) Aitken, Z. H.; Huang, R. Effects of Mismatch Strain and Substrate Surface Corrugation on Morphology of Supported Monolayer Graphene. *J. Appl. Phys.* **2010**, *107*, 123531.
(43) Stomp, R.; Miyahara, Y.; Schaer, S.; Sun, Q.; Guo, H.; Grütter, P.; Studenikin, S.; Poole, P.; Sachrajda, A. Detection of Single-Electron Charging in an Individual InAs Quantum Dot by Noncontact Atomic-Force Microscopy. *Phys. Rev. Lett.* **2005**, *94*, 056802.
(44) Tekiel, A.; Miyahara, Y.; Topple, J. M.; Grütter, P. Room-Temperature Single-Electron Charging Detected by Electrostatic Force Microscopy. *ACS Nano* **2013**, *7*, 4683−4690.
(45) Hong, I.-P.; Brun, C.; Pivetta, M.; Patthey, F.; Schneider, W.-D. Coulomb Blockade Phenomena Observed in Supported Metallic Nanoislands. *Front. Phys.* **2013**, *1*, 13.
(46) Cockins, L.; Miyahara, Y.; Bennett, S. D.; Clerk, A. A.; Studenikin, S.; Poole, P.; Sachrajda, A.; Grütter, P. Energy Levels of Few-Electron Quantum Dots Imaged and Characterized by Atomic Force Microscopy. *Proc. Natl. Acad. Sci. U. S. A.* **2010**, *107*, 9496−9501.
(47) Woodside, M. T. Scanned Probe Imaging of Single-Electron Charge States in Nanotube Quantum Dots. *Science* **2002**, *296*, 1098−1101.
(48) Kisiel, M.; Brovko, O. O.; Yildiz, D.; Pawlak, R.; Gysin, U.; Tosatti, E.; Meyer, E. Mechanical Dissipation from Charge and Spin Transitions in Oxygen-Deficient $SrTiO_3$ Surfaces. *Nat. Commun.* **2018**, *9*, 2946.
(49) Waser, R. *Nanoelectronics and Information Technology: Advanced Electronic Materials and Novel Devices*; Wiley VCH Verlag GmbH, 2012.
(50) Crowley, J. M. Simple Expressions for Force and Capacitance for a Conductive Sphere Near a Conductive Wall. *Proceedings of the ESA Annual Meeting on Electrostatics*; Minneapolis, MN, June 17−19, 2008; D1.
(51) Hudlet, S.; Saint Jean, M.; Roulet, B.; Berger, J.; Guthmann, C. Electrostatic Forces Between Metallic Tip and Semiconductor Surface. *J. Appl. Phys.* **1995**, *77*, 3308−3314.
(52) Hudlet, S.; Saint Jean, M.; Guthmann, C.; Berger, J. Evaluation of the Capacitive Force Between an Atomic Force Microscopy Tip and a Metalic Surface. *Eur. Phys. J. B* **1998**, *2*, 5−10.
(53) Elias, G.; Glatzel, T.; Meyer, E.; Schwarzman, A.; Boag, A.; Rosenwaks, Y. The Role of the Cantilever in Kelvin Probe Force Microscopy Measurements. *Beilstein J. Nanotechnol.* **2011**, *2*, 252−260.
(54) Preobrajenski, A. B.; Ng, M. L.; Vinogradov, N. A.; Vinogradov, A. S.; Lundgren, E.; Mikkelsen, A.; Martensson, N. Impact of Oxygen Coadsorption on Intercalation of Cobalt Under the h-BN Nanomesh. *Nano Lett.* **2009**, *9*, 2780−2787.
(55) Brugger, T.; Ma, H.; Iannuzzi, M.; Berner, S.; Winkler, A.; Hutter, J.; Osterwalder, J.; Greber, T. Nanotexture Switching of Single-Layer Hexagonal Boron Nitride on Rhodium by Intercalation of Hydrogen Atoms. *Angew. Chem., Int. Ed.* **2010**, *49*, 6120−6124.
(56) Muntwiler, M.; Zhang, J.; Stania, R.; Matsui, F.; Oberta, P.; Flechsig, U.; Patthey, L.; Quitmann, C.; Glatzel, T.; Widmer, R.; et al. Surface Science at the PEARL Beamline of the Swiss Light Source. *J. Synchrotron Radiat.* **2017**, *24*, 354−366.
(57) Li, X.-R.; Kong, F.-Y.; Liu, J.; Liang, T.-M.; Xu, J.-J.; Chen, H.-Y. Synthesis of Potassium-Modified Graphene and its Application in Nitrite-Selective Sensing. *Adv. Funct. Mater.* **2012**, *22*, 1981−1988.
(58) Chua, C. K.; Pumera, M. Renewal of sp^2 Bonds in Graphene Oxides *via* Dehydrobromination. *J. Mater. Chem.* **2012**, *22*, 23227−23231.
(59) Chun, K.-Y.; Lee, C. J. Potassium Doping in the Double-Walled Carbon Nanotubes at Room Temperature. *J. Phys. Chem. C* **2008**, *112*, 4492−4497.
(60) Mazov, I.; Krasnikov, D.; Stadnichenko, A.; Kuznetsov, V.; Romanenko, A.; Anikeeva, O.; Tkachev, E. Direct Vapor-Phase Bromination of Multiwall Carbon Nanotubes. *J. Nanotechnol.* **2012**, *2012*, 1−5.
(61) Wolloch, M.; Levita, G.; Restuccia, P.; Righi, M. Interfacial Charge Density and its Connection to Adhesion and Frictional Forces. *Phys. Rev. Lett.* **2018**, *121*, 026804.
(62) Giannozzi, P.; Baroni, S.; Bonini, N.; Calandra, M.; Car, R.; Cavazzoni, C.; Ceresoli, D.; Chiarotti, G. L.; Cococcioni, M.; Dabo, I.; et al. QUANTUM ESPRESSO: A Modular and Open-Source Software Project for Quantum Simulations of Materials. *J. Phys.: Condens. Matter* **2009**, *21*, 395502.

DOI: 10.1021/acsnano.9b00278
ACS Nano 2019, 13, 5485−5492